IEEE Access
Multidisciplinary ⋮ Rapid Review ⋮ Open Access Journal

Received 16 June 2023, accepted 15 July 2023, date of publication 20 July 2023, date of current version 27 July 2023.

Digital Object Identifier 10.1109/ACCESS.2023.3297486

RESEARCH ARTICLE

Nonlinear Stability Investigation of Type-4 Wind Turbines With Non-Autonomous Behavior Based on Transient Damping Characteristics

SUJAY GHOSH[1], (Graduate Student Member, IEEE), MOHAMMAD KAZEM BAKHSHIZADEH[1], GUANGYA YANG[2], (Senior Member, IEEE), ŁUKASZ KOCEWIAK[1], (Senior Member, IEEE), BIKASH C. PAL[3], (Fellow, IEEE), AND MITHULAN NADARAJAH[4], (Senior Member, IEEE)

[1]Ørsted Wind Power A/S, 7000 Fredericia, Denmark
[2]Department of Wind and Energy Systems, Technical University of Denmark, 2800 Kongens Lyngby, Denmark
[3]Department of Electrical and Electronic Engineering, Imperial College London, South Kensington, SW7 2BX London, U.K.
[4]School of Electrical Engineering and Computer Science, The University of Queensland, St Lucia, QLD 4072, Australia

Corresponding author: Sujay Ghosh (sujgh@orsted.com)

ABSTRACT As wind and solar power penetration increases, more and more conventional power plants are being replaced; as a result, the nature of transient stability of the system evolves where the converter's behaviour play dominating role during network events. This has necessitated a re-assessment of the nonlinear stability of the system. So far, the energy function-based transient stability method applied to synchronous machines has been applied to the converter-based system. However, there is ambiguity in terms of the damping quantification capturing the non-autonomous behaviour of the wind turbine systems, such as post-fault active current ramp rate control. This work aims to clarify the similarity between the synchronous machine model and a reduced large signal model of a wind turbine, and the difference in terms of the damping characteristics and how this impacts the system's stability from a nonlinear perspective. A non-autonomous energy function is discussed that analytically proves that a wind turbine system with post-fault active ramp rate control is more stable compared to no ramp rate control. Finally, the stability boundary (region of attraction) is constructed and validated using time-domain simulation studies in PSCAD.

INDEX TERMS Non-autonomous systems, wind turbine converter system, PLL, transient stability assessment, energy function, Lyapunov direct method.

I. INTRODUCTION

Presently there is about 743 GW of installed wind power capacity worldwide, reducing 1.1 billion tonnes of CO2 emissions globally [1]. Through technology innovations and economies of scale, the global wind power market has nearly quadrupled over the past decade and established itself as one of the most cost-competitive and resilient power sources worldwide [2]. Growth in the wind industry is expected to remain strong considering the policy support in the majority of the world, where various types of policy are driving capacity growth, including auctions, feed-in tariffs and renewable energy portfolio standards.

As wind and solar power penetration increases, more and more conventional power plants are being replaced; as a result, the power system operators are concerned about their systems' stable and reliable operation. An AC power system is a complex system which is vulnerable to disturbances, however, the generation must not be lost due to temporary disturbances of voltage or frequency. Traditionally, the stability of windfarms has been analysed through linearised model-based approach, such as eigenvalue analysis [3], [4], [5] or impedance-based stability analysis [6], [7], [8]. Wherein two types of instability events have been reported, such as the interaction between converter controls, and the interaction

The associate editor coordinating the review of this manuscript and approving it for publication was Ning Kang.

This work is licensed under a Creative Commons Attribution 4.0 License. For more information, see https://creativecommons.org/licenses/by/4.0/

between converter control and the AC grid. Nevertheless, such methods assume the entire system, including the wind turbine (WT) and the connected power system, has a linear behaviour under small disturbances, and stability is only analysed within the vicinity of the operating point, i.e. local stability is investigated.

On the other hand, a nonlinear approach to stability (transient stability) includes the assessment of large-signal disturbance and can provide global asymptotic stability conclusions. It has been proven that the transient stability of the WT system is mainly affected by the destabilisation of the phase-locked loop (PLL) under large disturbances in a weaker network [9]. Traditionally, transient stability has been assessed by running batches of time-domain simulations because of the lack of a closed-form solution for quantifying the stability margins, i.e. post-disturbance region of attraction (ROA) [10].

Conversely, analytical transient stability methods such as Lyapunov's direct method [11] are the main alternative to simulation-based methods since it provides an analytical representation of the system's stability property. Herein an energy function is constructed, such that post-disturbance, a decrease in energy will result in the state trajectories converging at an equilibrium point. As per literature, a classical energy function for synchronous generators is constructed based on its swing equation (autonomous differential equation) [12]. Some efforts have been made to extend the same analysis to WT systems [13]; however, the system is assumed to be autonomous. Generally, WT models exhibit non-autonomous system behaviour, i.e. the converter currents, the grid voltage, and the grid frequency are not necessarily time-invariant during the synchronisation event. For example, as per grid code requirements [14], the post-fault active current must be ramped up slowly, i.e. the post-fault active current is time-dependent; if an autonomous behaviour is assumed, then the post-fault active current is a constant. Therefore, assuming an autonomous WT model would result in an unrealistic analysis of the system's behaviour. As per the authors' knowledge, no research on energy-based transient stability investigations has been carried out for non-autonomous WT converter systems, and this gap has been discussed in our earlier work [15].

Due to unavailability, black-boxed, or computationally heavy EMT WT models, simplified reduced-order models (ROMs) resembling the actual system behaviour have gained prominence in stability studies. In general, the WT ROMs in [16], [17], [18], [19] address some nonlinear characteristics, such as low-frequency PLL dynamics and the impact of weak grids on the transient system behaviour. However, the non-autonomous system behaviour is not fully reflected. In our earlier work [20], an improved ROM has been proposed that considers a systematic approach to modelling the WT during faults considering the non-autonomous system behaviour.

This work extends our research on nonlinear modelling, and transient stability assessment of wind power plants (WPPs) [15], [20], [21]. The following is the contribution of the paper,

1) A tighter constraint on the stable equilibrium points for a system is proposed, wherein, unlike existing constraints, the proposed constraint is dependent on the PLL control.
2) A perspective on transient WT damping characteristics is presented, showing that during transients, the damping could be both positive or negative, influencing the system stability boundary.
3) An energy function for non-autonomous WT converter control systems (Type-4) is presented. The discussion shows that a non-autonomous energy function is needed since the ROA obtained from the non-autonomous model is likely to be larger than that of an autonomous model.

Section II presents the system modelling, discusses the classical swing equation for synchronous generators, and presents the equivalent swing equation for WTs with autonomous and non-autonomous system behaviour. Section III presents the WT system's energy-based transient stability assessment methodology. Section IV verifies the proposed energy-based stability assessment through time domain simulations. Finally, Section V presents the conclusion.

II. SYSTEM MODELING

For a synchronous generator (SG) represented by a constant voltage behind transient reactance, its motion is governed by the differential equations,

$$\begin{cases} M\dot{\omega} = T_m - T_e - D\omega \\ \dot{\delta} = \omega \end{cases} \tag{1}$$

where, δ is the voltage angle behind transient reactance, indicative of the generator's rotor position; ω is the rotor speed; M is the generator inertia constant; D is the damping coefficient. Both M and D are positive constants. T_m and T_e are the mechanical torque supplied by the alternator's prime mover and electrical torque output, respectively.

Equation (1) is often referred to as the swing equation. When stability analysis for SG is conducted using (1), it is customary to neglect the damping since it is not as important during the first swing transient, as it has a negligible effect on the magnitude of the swing. Furthermore, when synchronism is maintained in the first swing, damping is assumed to reduce the subsequent swings.

A. EQUIVALENT SWING EQUATION OF WTs

In earlier works [15], [20], and [21], it was discussed that during grid faults, a type-4 WT could be reduced to a grid-side converter with a constant DC voltage (as seen in Fig. 1a). As a result, the converter is just a current controlled source (as seen in Fig. 1b), wherein the current references are obtained from relevant grid codes [14]. Furthermore, the fast inner current control dynamics can be neglected when analysing the

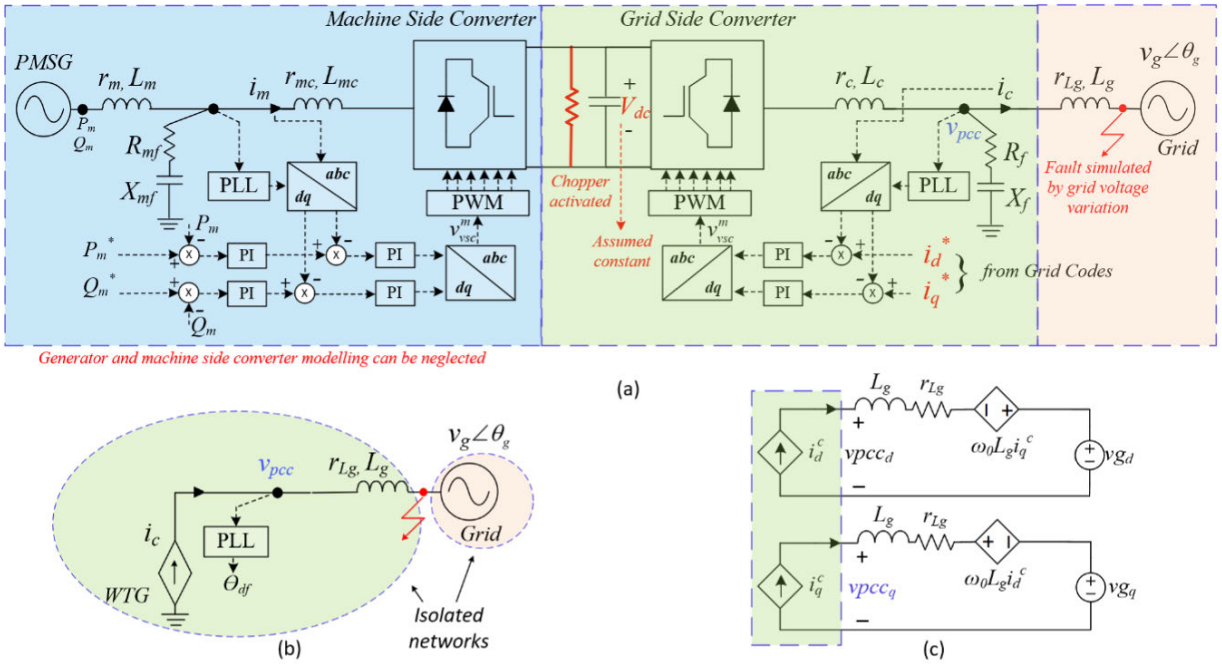


FIGURE 1. Wind turbine model: (a) Full topology of Type-4 wind turbine system, highlighting the actions/assumptions during faults. (b) Reduced order model (ROM) of the Type-4 wind turbine considering the actions/assumptions. Also showing the synchronisation instability of wind turbine systems during grid faults. (c) System representation of ROM in the DQ domain.

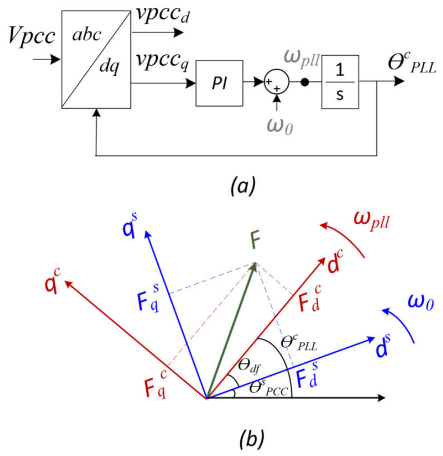


FIGURE 2. (a) SRF PLL control structure, (b) Frame misalignment between the system reference frame (dq^s) and converter reference frame (dq^c). The system in DQ frame rotates at a fixed frequency ω_0, where ω_g is the grid frequency.

slow PLL dynamics for large-signal stability analysis. In [20], it was also shown that the impact of the shunt capacitor filter on the stability could be neglected when the current is controlled on the grid-side LCL filter. A reduced-order representation of the WT in the DQ domain is illustrated in Fig. 1c. For synchronisation, an SRF PLL (shown in Fig. 2) is considered.

The equivalent swing equation of the WT converter system derived in [20] can be presented as,

$$M_{eq}\ddot{\delta} = T_{m_{eq}} - T_{e_{eq}} - D_{eq}\dot{\delta} \tag{2}$$

where,

$$\begin{aligned} M_{eq} &= 1 - k_p L_g i_d^c \\ T_{m_{eq}} &= k_p(\dot{\overline{r_{Lg} i_q^c}} + \ddot{\overline{L_g i_q^c}} + \dot{\overline{L_g i_d^c}}\omega_g) + k_i(r_{L_g} i_q^c \\ &\quad + \dot{\overline{L_g i_q^c}} + L_g i_d^c \omega_g) \\ T_{e_{eq}} &= (k_i V_g \sin\delta + k_p \dot{V}_g \sin\delta) + M\dot{\omega}_g \\ D_{eq} &= k_p(V_g \cos\delta - \dot{\overline{L_g i_d^c}}) - k_i L_g i_d^c \end{aligned} \tag{3}$$

where, k_p and k_i are the PLL controller gains, i_d^c and i_q^c are the converter currents in converter reference frame, r_{Lg} and L_g are the grid impedance, V_g and ω_g is the grid voltage and frequency. It must be noted that the WT system is modelled in a DQ frame, rotating at a fixed frequency ω_0. The WT model described in (2) is a second-order nonlinear damped differential equation that considers the time variance of the system parameters represented by the derivatives in (3).

From (1) and (2), it is observed that WTs share a similarity with SGs in terms of the mathematical model describing synchronisation dynamics during grid disturbances. Similar to SGs, the synchronisation dynamics of WTs are affected by the torque deviation ($T_m - T_e$). However, unlike SGs, the damping coefficient D_{eq} is not a constant and cannot be ignored since it depends on the PLL angle δ, and could be negative. Since transient stability is a post-disturbance stability problem, for a post-fault scenario, the model (2) can be adapted into two variants: (a) simplified nonlinear autonomous system, e.g. dy/dt = f(y); and (b) nonlinear non-autonomous system, e.g. dy/dt = f(t,y).

1) AUTONOMOUS WT MODEL

In (2), all the post-fault time-varying system parameters (i.e. $\dot{i}_d^c$, $\dot{i}_q^c$, $\dot{V}_g$ and $\dot{\omega}_g$) are neglected, as a result, (2) can be simplified into a simple nonlinear autonomous system (4). Considering the assumption, a drawback of this model variant is that it cannot simulate the post-fault active current recovery ramp rate needed for enhanced WT system stability. Instead, a jump (step response) in post-fault active current is considered,

$$\begin{aligned} \dot{x_1} &= x_2 \\ M'\dot{x_2} &= T'_m - T'_e(x_1) - D'(x_1)\cdot x_2 \end{aligned} \tag{4}$$

where, $x_1 = \delta$ and $x_2 = \dot{\delta}$,

$$\begin{aligned} M' &= 1 - k_p L_g i_d^c \\ T'_m &= k_i(r_{L_g} i_q^c + L_g i_d^c \omega_g) \\ T'_e(x_1) &= k_i V_g \sin x_1 \\ D'(x_1) &= k_p V_g \cos x_1 - k_i L_g i_d^c \end{aligned} \tag{5}$$

2) NON-AUTONOMOUS WT MODEL

Here, all the post-fault time-varying system parameters except $\dot{i}_d^c$ are neglected, as a result, (2) can be simplified into (6) which is a nonlinear non-autonomous system. When $\dot{i}_d^c$ is a constant, it resembles the post-fault active current recovery ramp rate (i.e. $\dot{i}_d^c = i_d^{c,ramp}$). Then $i_d^c = (i_d^{c,ramp} t + i_{d0}^c)$ is replaced in (2), where i_{d0}^c is the active current injected during the fault.

$$\begin{aligned} \dot{x_1} &= x_2 \\ M''(t)\dot{x_2} &= T''_m(t) - T''_e(x_1) - D''(t, x_1)x_2 \end{aligned} \tag{6}$$

where,

$$\begin{aligned} M''(t) &= 1 - k_p L_g (i_d^{c,ramp} t + i_{d0}^c) \\ T''_m(t) &= k_p (L_g i_d^{c,ramp} \omega_g) + k_i (r_{L_g} i_q^c \\ &\quad + L_g (i_d^{c,ramp} t + i_{d0}^c)\omega_g) \\ T''_e(x_1) &= k_i V_g \sin x_1 \\ D''(t, x_1) &= k_p (V_g \cos x_1 - L_g i_d^{c,ramp}) - k_i L_g (i_d^{c,ramp} t + i_{d0}^c) \end{aligned} \tag{7}$$

This model simplification is slightly complex but realistic in representing standard post-fault active current. Table 1 presents the parameters describing the WT system considered in this study.

III. TRANSIENT STABILITY ASSESSMENT METHODOLOGY

The existence of an equilibrium point is a prerequisite for the transient stability of a post-disturbed system. This section presents a tighter constraint on the equilibrium points based on small signal stability analysis and further presents an energy-function-based transient stability assessment of a WT converter system.

TABLE 1. System and control parameters [22].

Symbol	Description	Value
S_b	WT Rated power	1x12 MVA
V_g	Nominal grid voltage (L-N, pk)	690 $\sqrt{2/3}$ V
f_g	Rated frequency	50 Hz
r_{Lg}, L_g	Grid-side impedance	SCR=3.3, X/R=16.3
i_d^c, i_q^c	Pre-disturbance active and reactive currents (pu)	1.0, -0.1
K_{pll}	SRF PLL design: k_p k_i	0.005, 1.5
$i_d^{c,ramp}$	Post fault active current ramp rate	2.84 kA/s, and 28.4 kA/s

The PLL gains are chosen to obtain a slow PLL bandwidth.

A. CONSTRAINTS ON EQUILIBRIUM POINTS

At steady state, the system (2) can be rewritten in ODE form as,

$$\begin{bmatrix} \dot{x_1} \\ \dot{x_2} \end{bmatrix} = \begin{bmatrix} x_2 \\ \frac{1}{M_{eq}}(T_{m_{eq}} - T_{e_{eq}}(x_1) - D_{eq}x_2) \end{bmatrix} \tag{8}$$

There are two equilibrium points (when $T_{m_{eq}} = T_{e_{eq}}$) for the dynamical systems,

$$\tilde{x}_1 = \begin{bmatrix} \sin^{-1}(\gamma) \\ 0 \end{bmatrix} \text{and } \tilde{x}_2 = \begin{bmatrix} \pi - \sin^{-1}(\gamma) \\ 0 \end{bmatrix} \tag{9}$$

where $\gamma = (r_{Lg} i_q^c + L_g \omega_g i_d^c)/V_g$

It is worth noting that $\sin^{-1}x$ is defined for $|\ x\ | \leq 1$ in $\mathbb{R}$. This gives a static constraint on the steady-state operating point, as shown in (10). In other words, (10) shows whether the desired operating point is reachable from a load flow perspective (no controller gains are present).

$$|\ \gamma\ | \leq 1 \implies \ |\ \frac{r_{Lg} i_q^c + L_g \omega_g i_d^c}{V_g}\ | \leq 1 \tag{10}$$

Initially, to obtain the system (2), a fast current controller dynamics compared to the PLL dynamics was considered, ensuring no interaction between the two controllers. However, there could be an interaction between the PLL and the AC grid.

Linearisation of (8) around $\tilde{x}$, gives

$$\begin{aligned} A &= \frac{\partial f}{\partial x}|_{x=\tilde{x}} \\ &= \begin{bmatrix} 0 & 1 \\ \frac{\mp k_i V_g}{1 - k_p L_g i_d^c}\sqrt{1-\gamma^2} & \frac{k_i L_g i_d^c \mp k_p V_g \sqrt{1-\gamma^2}}{1 - k_p L_g i_d^c} \end{bmatrix} \end{aligned} \tag{11}$$

To have small-signal stability, **A** must be a Hurwitz matrix, where the real part of all its eigenvalues should be negative. If the Routh-Hurwitz criterion is applied to the characteristic equation of **A**, then (12) must be satisfied to have a stable equilibrium point. This constraint puts a tighter restriction on the stable steady-state angle $\tilde{x}_1$ (considering PLL gains) and also determines that $\tilde{x}_2$ is unstable. In (12), $\mp$ indicates $\tilde{x}_1$ and $\tilde{x}_2$ is obtained through subtraction and addition, respectively.

$$\begin{cases} \frac{1}{1 - k_p L_g i_d^c}(k_i L_g i_d^c \mp k_p V_g \sqrt{1-\gamma^2}) < 0 \\ \frac{\mp k_i V_g}{1 - k_p L_g i_d^c}\sqrt{1-\gamma^2} < 0 \end{cases} \tag{12}$$

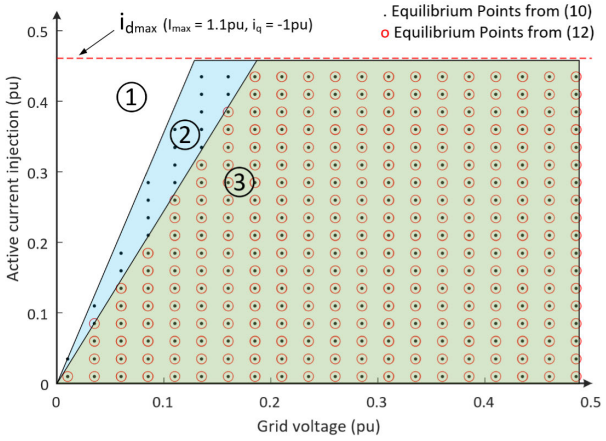


FIGURE 3. Steady-state i_d injection with change in V_g (based on Table 1); ①: Unstable region; ②∪③: Stable region as per (10); ③: Stable region as per (12).

During severe grid faults, considering a converter current rating I_{max} = 1.1p.u. and i_q = -1.0p.u. (as per [14], for severe voltage drop, i.e. less than 0.5 p.u., i_q = -1.0p.u. must be injected), the steady-state i_d can be solved, using (10) or (12), at each point of grid voltage $V_g \in [0, 0.5]$ p.u., as shown in Fig. 3. During faults, the equilibrium points obtained from the static constraint (10) are depicted by the region ②∪③. Whereas the equilibrium points obtained from the proposed tighter constraint (12) are depicted by region ③.

From Fig. 3, an important observation is that when the system damping increases, the stable region obtained from the proposed tighter constraint (12) tends to the stable region obtained from the static constraint (10). Hence, it can be concluded that the proposed equation (12) provides a tighter constraint on the i_d injection, guaranteeing a small-signal stable system.

B. TRANSIENT DAMPING CHARACTERISTICS

The objective of the damping coefficient D_{eq} in (2) is to obtain negative feedback. For instance, when ω_{pll} is larger than ω_g, then positive D_{eq} ensures a negative rate change of ω_{pll} to aid the decrease of ω_{pll}, and vice versa. Hence, a positive damping coefficient is helpful to the transient stability. However, as seen in (2), D_{eq} is affected by the PLL angle, therefore, positive D_{eq} cannot be guaranteed during the transients. When δ is outside a certain range $(\delta_{min}, \delta_{max})$, D_{eq} becomes negative endangering transient stability. Later in the paper, the range $(\delta_{min}, \delta_{max})$ is computed.

Fig. 4 shows an example of the $D_{eq}(\delta)$ trajectory during transients. As long as D_{eq} is positive, i.e. δ is within the $(\delta_{min}, \delta_{max})$, the system is strictly stable (purple region). The red boundary corresponds to the locus of unstable points beyond which the trajectory can never converge to its stable equilibrium point, i.e. the system will be strictly unstable. The orange region corresponds to the negative damping region, wherein if it enters, the trajectory could be stable or unstable [23]. It is clearly seen that considering a strictly positive D_{eq} may lead to a conservative analysis of the system

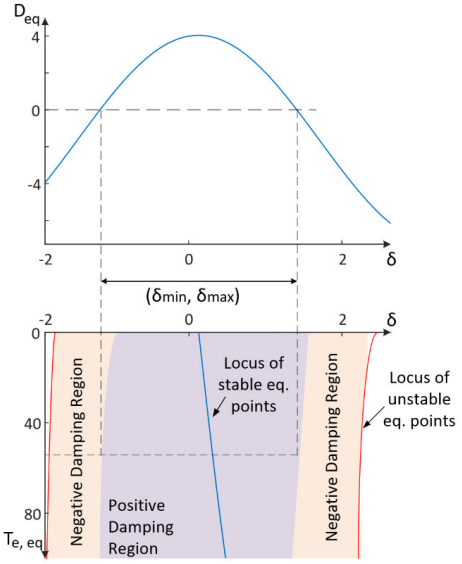


FIGURE 4. Distribution diagram of the nonlinear damping term D_{eq} in (2).

stability boundary. However, considering the same is a sufficient condition for system stability. It may be pointed out that not many existing literature reports the dependency of post-fault active current ramp rate on transient damping. This is particularly important when analysing the post-fault system characteristics.

C. LARGE SIGNAL ANALYSIS

Even if a system is small signal stable, it may become unstable due to poor transient behaviour. Energy-based approaches have been successfully applied to analyse the rotor-angle transient stability of synchronous generators, and the same could be extended to WT systems having an equivalent swing equation. In this section, the energy function for various models is discussed.

Assuming the post-disturbance system $f(x)$ has a stable equilibrium at x_0. Then the system is locally asymptotically stable in the region of attraction (ROA) $\mathbb{A}(x_0)$ if an energy function $V(x)$ exists such that,

$$V(x) > 0, V(x_0) = 0, \dot{V}(x) = \nabla V(x) \cdot f(x) \leq 0 \qquad (13)$$

Analytically, it is difficult to obtain the exact $\mathbb{A}(x_0)$. Instead, several stability assessment methods try to find a relaxed set defined as,

$$\mathbb{A}_\beta(x_0) = \mathbb{A}(x_0) \cap \{x | V(x) \leq \beta\} \qquad (14)$$

where β is a positive constant that determines the boundary of $\mathbb{A}_\beta(x_0)$ [24].

1) ENERGY FUNCTION FOR SYNCHRONOUS GENERATORS

For SGs described by (1), the standard energy-function as per literature [12] can be constructed as,

$$V_{SG}(\delta, \omega) = M \int_0^t \omega\dot{\omega}(t)dt - \int_0^t \omega(T_m - T_e)dt$$

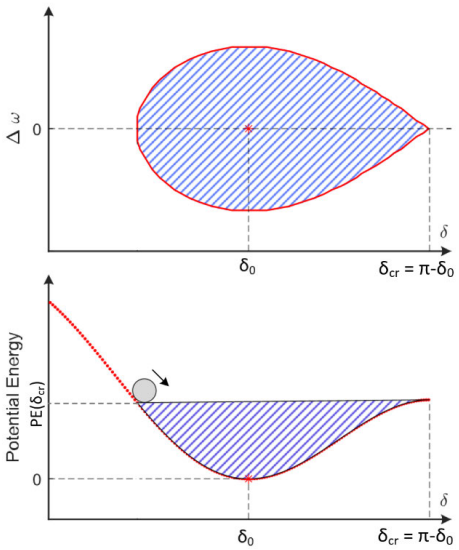


FIGURE 5. Synchronous generator: Stability boundary and potential energy surface based on the energy function V_{SG}.

$$= 0.5\, M(\omega_t^2 - \omega_0^2) + \int_{\delta_0}^{\delta_t} (T_e(\delta) - T_m)d\delta$$
$$= KE(\omega) + PE(\delta) \tag{15}$$
$$\dot{V}_{SG}(\delta, \omega) = -\omega^2 D = 0 \text{ (damping neglected)} \tag{16}$$

If the system is to remain stable following a disturbance, the energy must always be positive except at the equilibrium point $x_0 = (\delta_0, 0)$ where it is zero, $\dot{V}_{SG}(\delta, \omega) \leq 0$, and the energy of the disturbed system must not exceed a critical level $\beta = PE(\delta_{cr})$, as described in (14). From [25], $\delta_{cr} = \pi - \delta_0$. For example, in Fig. 5, the region enclosed by $PE(\delta_{cr})$ is the estimated ROA (red dotted); therefore, as long as the ball is within δ_{cr}, the system will be stable, i.e. once the ball crosses δ_{cr}, it can never come back to its stable equilibrium point δ_0.

2) ENERGY FUNCTION FOR AUTONOMOUS WT MODEL

Considering the fact that the WT model (4) is an autonomous differential equation, its energy function can be constructed similarly to (15). For post-disturbance equilibrium point $(x_{1,0}, x_{2,0} = 0)$ the energy function obtained is,

$$V_A(x) = M' \int_0^t x_2 \dot{x}_2 dt - \int_0^t x_2(T'_m - T'_e)dt$$
$$= 0.5\, M' x_{2,t}^2 - k_i V_g \left[\cos(x_{1,t}) - \cos(x_{1,0})\right]$$
$$- \left[k_i(Ri_q^c + L_g i_d^c \omega_n)\right](x_{1,t} - x_{1,0})$$
$$= KE(x_2) + PE(x_1) \tag{17}$$
$$\dot{V}_A(x) = -x_{2,t}^2 D'$$
$$= -x_{2,t}^2 [k_p V_g \cos(x_{1,t}) - k_i L_g i_d^c] \tag{18}$$

Therefore, for $\dot{V}_A(x) \leq 0$, the dissipativity condition ($D' \geq 0$) has to be satisfied. The range $(\delta_{min}, \delta_{max})$ at which $D' \geq 0$

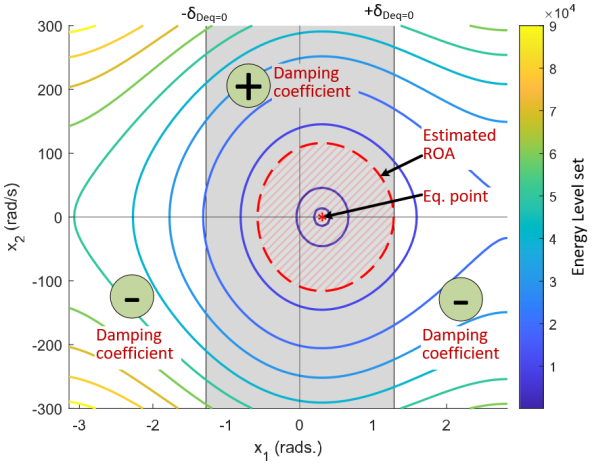


FIGURE 6. Autonomous WT model: Stability boundary based on the energy function V_A.

can be calculated by solving,

$$\delta_{D'=0} = cos^{-1}\left(\frac{k_i L_g i_d^c}{k_p V_g}\right) \tag{19}$$

For the system (4), a sample energy contour plot $V_A(x)$ is illustrated in Fig. 6. The energy is always positive except at the equilibrium point $(x_{1,0}, 0)$, where it is zero. However, $\dot{V}_A(x) \leq 0$ is only guaranteed in the grey region. The estimated ROA for the autonomous WT model is the energy level set that touches $\delta_{cr} = +\delta_{D'=0}$.

3) ENERGY FUNCTION FOR NON-AUTONOMOUS WT MODEL

For stable operation, many grid codes [14] require a slow post-fault active current ramp rate. Unlike the autonomous WT model (4), the energy function for the non-autonomous model (6) cannot be constructed similarly to the energy function for SGs, since, in (6), the post-fault active current varies over time.

In 1974, Baker [26] established some sufficient conditions that guarantee the uniform stability of a second-order nonlinear non-autonomous forced and damped system defined by,

$$\overline{r(t)\dot{u}} + \phi(t, u, \dot{u})\dot{u} + p(t)f(u) = h(t, u, \dot{u}) \tag{20}$$

with the equivalent system,

$$\dot{x} = y$$
$$\dot{y} = -[\dot{r}(t)y + \phi(t, x, y)y + p(t)f(x) - h(t, x, y)]/r(t) \tag{21}$$

where, under certain assumptions, the following energy function was proposed,

$$V_B(t, x, y) = exp(-E(t)) \cdot [2p(t)r(t)F(x) + [r(t)y]^2 + 1] \tag{22}$$

Since our proposed WT model is a second-order nonlinear non-autonomous system, (6) can be mapped onto (21), such

that $x = \delta$, $y = \dot{\delta}$, and

$$\begin{aligned} r(t) &= 1 - k_p L_g (i_d^{c,ramp} t + i_{d0}^c) = M'' \\ \dot{r}(t) &= -k_p L_g i_d^{c,ramp} \\ \phi(t,x,y) &= k_p V_g \cos x_1 - k_i L_g (i_d^{c,ramp} t + i_{d0}^c); \\ \dot{r}(t) + \phi(t,x,y) &= D'' \\ p(t) &= 1 \\ f(x) &= k_i V_g \sin x_1 = T_e'' \\ h(t,x,y) &= k_p L_g i_d^{c,ramp} \omega_g + k_i (r_{L_g} i_q^c \\ &\quad + L_g (i_d^{c,ramp} t + i_{d0}^c) \omega_g) = T_m'' \end{aligned} \tag{23}$$

The assumptions under which the energy function (22) was proposed must also hold in our model (6).

- $\lim_{t\to\infty} p(t)$ exists,
  In our model, $p(t) = 1$, therefore $\lim_{t\to\infty} p(t)$ always exists in $t \in [0, t]$.
- $\lim_{t\to\infty} r(t)$ exists,
  The current ramp is only applied for a limited time, and after the current reaches the final value it saturates, therefore $r(t) = 1 - k_p L_g (i_d^{c,ramp} t + i_{d0}^c)$ is always bounded in $t \in [0, t]$.
- $r_0 \le r(t) \le r_1$, for all $t \ge 0$, where r_0, r_1 are positive constants,
  In our model, $r(t) = M''$ which is always positive for our system design [13].
- $|\dot{r}(t)| \le \rho$, for all t ≥ 0,
  In our model, $\dot{r}(t) = -k_p L_g i_d^{c,ramp}$ which is a constant and therefore is always bounded in $t \in [0, t]$.
- $f(0) = 0$,
  In our model, $f(0) = k_i V_g \sin(0) = 0$.
- $F(x) \ge 0$, where $F(x) = \int_0^x f(s)ds$
  In our model,

$$\begin{aligned} F(x) &= \int_0^{x_1} [k_i V_g \sin x_1]\, dx_1 \\ &= -k_i V_g (cos(x_1) - 1) \ge 0, \forall\, x_1 \end{aligned} \tag{24}$$

- $\phi(t,x,y) \ge 0$, for all x, y and $t \in [0, t]$,
  As per (23), let

$$\begin{aligned} &\phi(t,x,y) = 0 \\ &k_p V_g \cos x_1 - k_i L_g (i_d^{c,ramp} t + i_{d0}^c) = 0 \\ &\cos x_1 = \frac{k_i L_g (i_d^{c,ramp} t + i_{d0}^c)}{k_p V_g} \\ &\hat{x}_1 = \cos^{-1}\Big(\frac{k_i L_g (i_d^{c,ramp} t + i_{d0}^c)}{k_p V_g}\Big) \end{aligned} \tag{25}$$

  To satisfy $\phi(t,x,y) \ge 0$, in our model $x_1 \in [-\hat{x}_1, +\hat{x}_1]$.
- $\phi(t,x,y) \ge k(x,y) \ge 0$, where, $k(x,y)$ is the damping coefficient for equivalent autonomous systems.
  This constraint gives a relation between the damping of a non-autonomous system against that of an equivalent autonomous system, where $\phi(t,x,y) \ge D'(x,y) \ge 0$.
- $xf(x) > 0$, for all $x \in R \setminus 0$,
  Since in our model, $x_1 \in [-\hat{x}_1, +\hat{x}_1]$, therefore $xf(x) = x_1 \cdot k_i V_g \sin(x_1) > 0$ for all $x_1 \in [-\hat{x}_1, +\hat{x}_1]$.
- $|h(t,x,y)| \le e(t)$; $(t,x,y) \in I \times R^2$,
  In our model $e(t) = |h(t,x,y)|$.
- $\lim_{t\to\infty} e(t)$ exists,
  In our model, since the current ramp saturates at the final value, therefore, $e(t)$ is always bounded in $t \in [0, t]$.
- $\lim_{t\to\infty} E(t) = E_0 < \infty$, where, $E(t) = \int_0^t e(s)ds$,
  In our model,

$$\begin{aligned} E(t) &= \int_0^t [k_p L_g i_d^{c,ramp} \omega_g + k_i (r_{L_g} i_q^c \\ &\quad + L_g (i_d^{c,ramp} t + i_{d0}^c) \omega_g)]\, dt \\ &= \frac{L_g k_i \omega_g i_d^{c,ramp} t^2}{2} + (r_{L_g} i_q^c k_i + L_g k_p \omega_g i_d^{c,ramp} \\ &\quad + L_g i_{d0}^c k_i \omega_g) t \end{aligned} \tag{26}$$

  Once again, since the current ramp saturates at the final value, $E(t)$ is always bounded in $t \in [0, t]$.

Since all the assumptions hold, the energy function (22) is a valid Lyapunov function for our WT model (6). Furthermore, it can easily be proved that (27) is the time derivative of (22),

$$\dot{V}_B(t,x,y) = -2r(t) exp(-E(t)) \phi(t,x,y) y^2 \tag{27}$$

As discussed in the assumptions, (a) $r(t)$ is always positive; (b) since $E(t)$ is bounded then $exp(-E(t))$ is always positive; (c) also, since $\phi(t,x,y)$ is positive in $[-\hat{x}_1, +\hat{x}_1]$, therefore, $\dot{V}_B(t,x,y)$ is always less than zero in $[-\hat{x}_1, +\hat{x}_1]$.

From (25), it may be observed that $\delta_{\phi=0}$ $(= \hat{x}_1)$ is time dependent; this makes the estimated ROA a function of time. To maximise the estimated ROA boundary, we must obtain its corresponding value of $\delta_{\phi=0}$. $\delta_{\phi=0}$ is maximum at the instant of fault clearance (i.e. t=0). However, at t=0, the impact of the current ramp rate is neglected; therefore, $\delta_{\phi=0}$ is suggested to be computed at time t=0^+. This presumption is true since the values of the states do not change much from t=0 to t=0^+. Furthermore, as t increases, the ROA reduces until the active current saturates. Therefore, the upper and lower bound of ROA is given, where the ramp rate determines how fast the ROA shrinks in the recovery phase. The slower it shrinks, the system is more stable. The same could be seen in the time domain simulations in Section IV.

For the system (6), a sample energy contour plot $V_B(x)$ is illustrated in Fig. 7 (with a ramp rate of 2.84 kA/s). The energy is always positive except at the equilibrium point (δ, 0), where it is zero. However, $\dot{V}_B(x) \le 0$ is only guaranteed in the grey region $[-\delta_{\phi=0}, +\delta_{\phi=0}]$. The estimated ROA is the energy level set that touches $\delta_{cr} = +\delta_{\phi=0}$.

4) ROA SENSITIVITY ANALYSIS

The area of the ROA provides an estimate of how stable the system is, i.e. a large ROA has a large stability margin. Fig. 8 presents the ROA sensitivity of the autonomous WT model (4) under high/ low damping and strong/ weak grid scenarios. As expected, based on visual inspection, the area of ROA for the low damping and weak grid scenario is the least, i.e. this scenario would be the least stable for the same grid disturbance applied to all the scenarios.

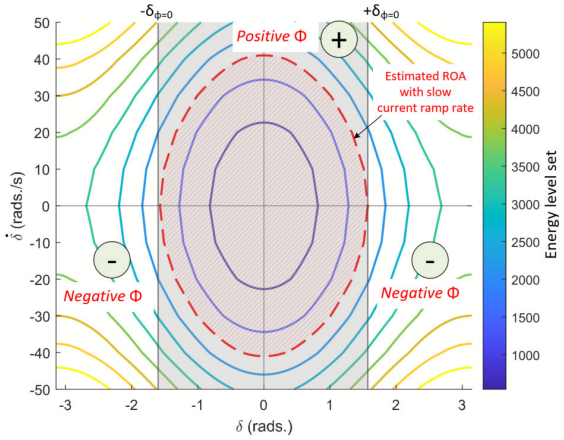


FIGURE 7. Non-autonomous WT model: Stability boundary based on energy function.

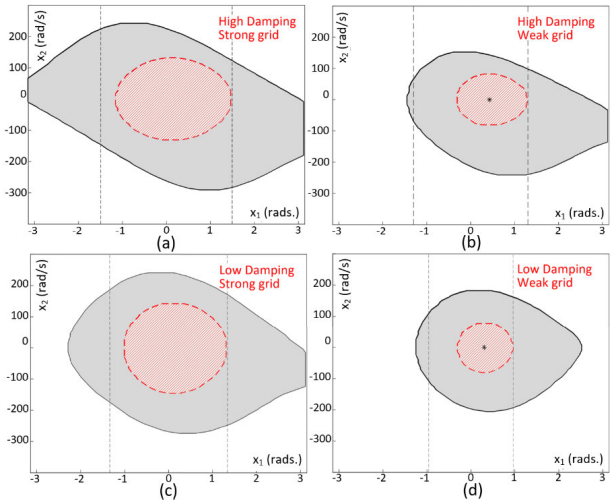


FIGURE 8. ROA of the autonomous WT model, (a) High damping and strong grid, (b) High damping and weak grid, (c) Low damping and strong grid, (d) Low damping and weak grid. The grey region is the exact ROA obtained from stable manifolds; the red region is the estimated ROA.

Furthermore, Fig. 9 presents the ROA sensitivity of the non-autonomous WT model (6) for a ramp rate of 2.84 kA/s and 28.4 kA/s, respectively. An important observation is that the ROA obtained for the system with slow current ramp rate control has a larger area when compared to the system with fast current ramp rate control. What this means is that a post-fault system with a slow current ramp rate is more stable than a system with fast current ramp rate control.

IV. TRANSIENT STABILITY – TIME DOMAIN VERIFICATION

This section verifies the analytically estimated nonlinear boundary, i.e., ROA for the WT reduced order model, against an EMT WT switching model in PSCAD.

A. NEED FOR NON-AUTONOMOUS WT MODEL AND ENERGY FUNCTION

As discussed in Section II, WT systems exhibit non-autonomous system behaviour, i.e. the system states are

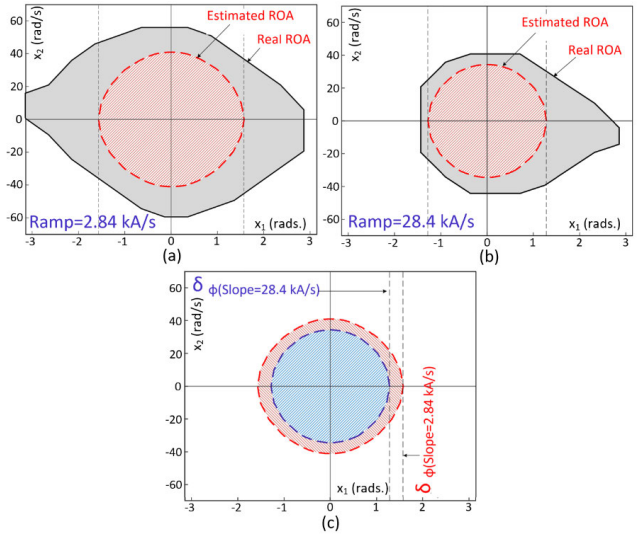


FIGURE 9. ROA of the non-autonomous WT model, (a) with a post-fault active current ramp rate of 2.84 kA/s, (b) with a post-fault active current ramp rate of 28.4 kA/s, (c) comparison of estimated ROA with fast current ramp rate (28.4 kA/s) against slow current ramp rate (2.84 kA/s). The grey region is the exact ROA obtained from stable manifolds; the red region is the estimated ROA.

not necessarily time-invariant during synchronisation. If an autonomous behaviour of the WT is assumed, it will lead to an unrealistic analysis of the system behaviour. For example, in Fig. 10, the time domain plots for an identical disturbance with no ramp rate control (autonomous model) and with ramp rate control (non-autonomous model) are presented, where it can be observed that the trajectory with autonomous behaviour is unstable. In contrast, the trajectory with non-autonomous behaviour is stable. This means that if an energy-based stability analysis of a WT system is carried out with the generally accepted energy function (considering autonomous behaviour), which does not consider ramp rate control, then an unrealistic analysis of the system's behaviour is obtained because, in reality, actual WT systems exhibit non-autonomous behaviour, which has a stable trajectory.

B. TIME DEPENDENT NON-AUTONOMOUS SYSTEM ROA BOUNDARY

As discussed in Section III, from (25), it may be recalled that $\delta_{\phi=0}$ $(= \hat{x}_1)$ is time dependent; this makes the estimated ROA, for the non-autonomous system, a function of time. The same can be observed from Fig. 11. Post fault, $\delta_{\phi=0}$ is maximum at t=0 and minimum when the active current ramp saturates. It may be recalled that to maximise the estimated ROA boundary, the time t=0$^+$ was proposed, presuming that the states' values do not change much from t=0 to t=0$^+$. This assumption is validated in Fig. 11, where in our calculations, t=0$^+$= 1 ms (post fault clearance).

C. ROA TIME DOMAIN VERIFICATION

The post-fault WT models with system parameters defined in Table 1 are simulated with various initial conditions (resulting from a grid voltage dip and varying fault clearing times).

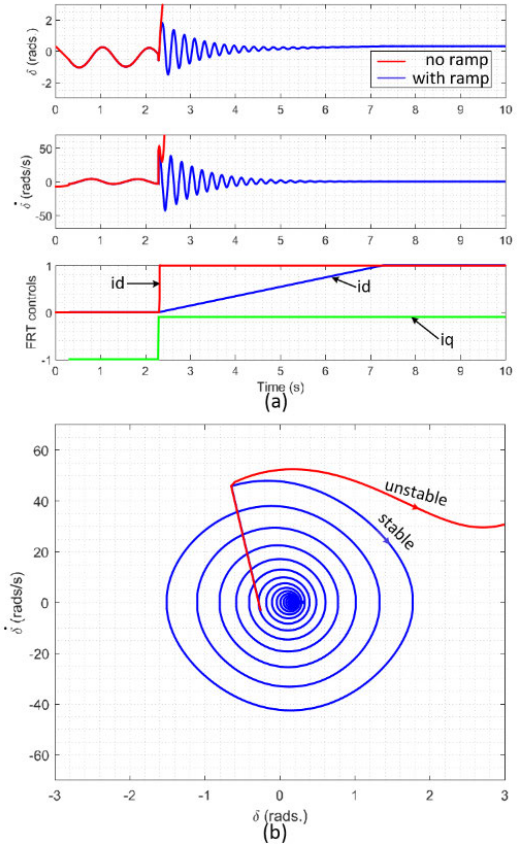


FIGURE 10. Post-fault clearance time-domain trajectory for an identical disturbance (V_g = 5% to 100%) of Non-autonomous system (with ramp) Vs autonomous system (no ramp). (a) Time trajectory, (b) Phase portrait.

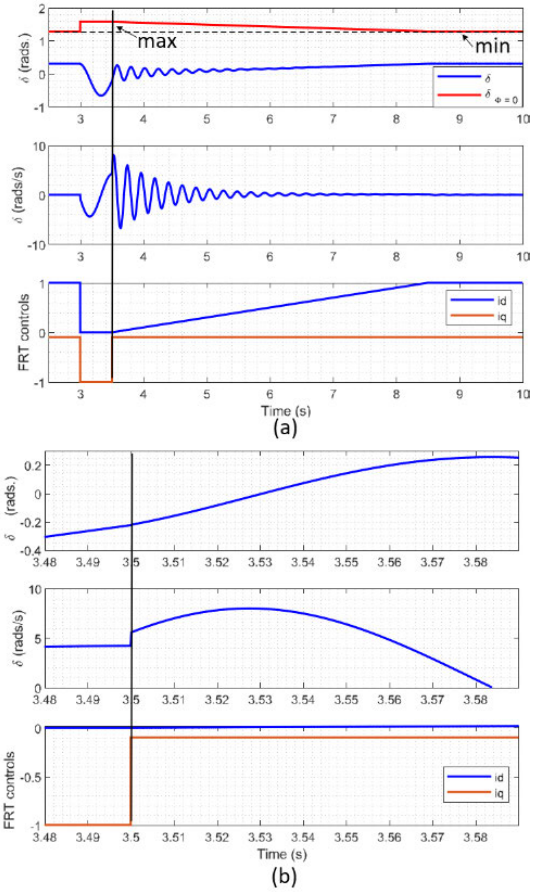


FIGURE 11. (a) Time-dependent ROA boundary for non-autonomous system $\delta_{\phi=0}$, (b) Zoomed in view for time-dependent non-autonomous system ROA boundary $\delta_{\phi=0}$.

1) AUTONOMOUS WT MODEL – NO ACTIVE CURRENT RAMP RATE

The fault ride through current references is presented in Fig. 12a (subfigure one), where it can be observed that there is no post-fault active current ramp. The two-dimensional phase portrait for the event simulated is presented in Fig 12a (subfigure two), and the analytically estimated ROA is also presented. It can be observed that post-fault, the initial point trajectory is inside the estimated ROA; as a result, as expected, the trajectory converges to the stable equilibrium point. Similarly, the energy trajectory for the simulated event is presented in Fig. 12a (subfigure three). Where it can be observed that the energy is always greater than or equal to zero. Also, since the initial point trajectory is inside the estimated ROA, the energy change rate is always less than or equal to zero ($t \geq 3.5$ s). Furthermore, a general observation is that since a step response on the post-fault active current is applied, the trajectories are highly oscillatory, i.e. it has a high settling time. It may be noted that since Lyapunov's direct method only provides sufficient conditions for stability, therefore only stable cases are presented.

2) NON-AUTONOMOUS WT MODEL – WITH ACTIVE CURRENT RAMP RATE

For an identical disturbance the system trajectories with two different post-fault active current ramp rates (28.4 kA/s and 2.84 kA/s) are presented in Fig. 12b and c, respectively. The two-dimensional phase portraits for the simulated events are presented in Fig 12b and c (subfigure two), and the estimated ROAs are also presented. Since the post-fault initial point trajectories are inside the estimated ROAs, the system converges to the stable equilibrium point. Simultaneously, the energy trajectories are always greater than or equal to zero, resulting in the energy rate change to be always less than or equal to zero. Furthermore, it is observed that, as expected, the system with 28.4 kA/s ramp rate is more oscillatory compared to the system with 2.84 kA/s ramp rate; however, they are less oscillatory compared to the autonomous system.

In general, it is seen that the estimated ROA for the non-autonomous system was larger than the ROA of an equivalent autonomous system; this is supported by the fact that for a post-fault scenario, a slow active current ramp rate ensures a more stable operation compared to a jump in the active current. This observation was also validated through time domain simulations. A limitation of the proposed energy function is that when the damping is very high for the system, the boundary $\delta_{\phi=0}$ tends to $\pm\pi/2$. As a result, the ROAs are always conservative. However, even with the conservative estimate of ROA, the results show that when the post-fault

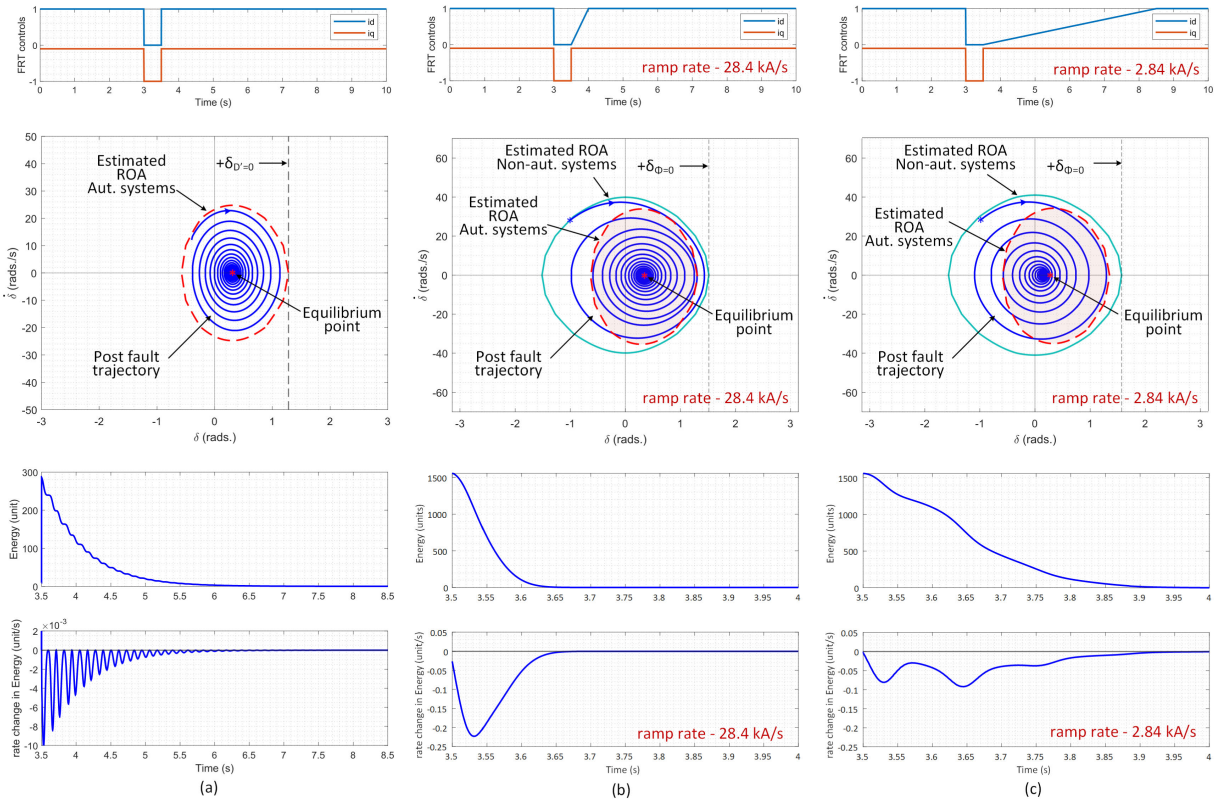


FIGURE 12. Time-domain simulations: (a) Converter states for autonomous WT system, (b) Converter states for non-autonomous WT system with a current ramp rate of 28.4 kA/s, (c) Converter states for non-autonomous WT system with a current ramp rate of 2.84 kA/s.

initial point trajectory is near the boundary, the system is oscillatory. Hence, estimating a larger boundary may not be beneficial as a more oscillatory response may not be valuable. This understanding is especially true when the ROA estimate is used to tune the PLL gains. Nevertheless, it is always nice to have a sharper system boundary; in light of this, it could be fruitful to consider the negative transient damping characteristics within the energy function for the WT system. While the primary focus of this work is on individual wind turbines. It must be noted that our proposed method has the potential for adaptability at the wind power plant (WPP) level as well, where the WPP with multiple WTs can be aggregated as a single machine equivalent, and this is a plausible future extension of our research.

Overall, the proposed energy function has high confidence in the application for transient stability investigation. The advantages are two-fold. Firstly, during the system modelling stage - the WT model need not be simplified to an autonomous system, which diminishes the characteristics of the transient behaviour of the original WT system. Secondly, for transient stability assessment, a larger ROA can be obtained, which gives a better estimate of the stability margin of the system.

V. CONCLUSION

This work extends our research on nonlinear modelling and transient stability assessment of wind power plants (WPPs) and presents a methodology for energy-based transient stability assessment of a non-autonomous type-4 WT system model. The following are the conclusions of the paper,

1) Based on the linear analysis, tighter constraints on the equilibrium points for a stable system are proposed, ensuring no interaction exists between the PLL and the AC grid. The model assumption of slow PLL bandwidth with respect to the current controller ensures that the current controller and the PLL does not interact. Hence, the methodology ensures the system is always small signal stable.
2) A small signal-stable system does not guarantee transient stability. In this regard, an energy-based transient stability assessment is carried out, wherein a non-autonomous energy function for a WT system is discussed, considering positive transient damping characteristics. It was shown that an energy function for non-autonomous WT systems is needed as the established energy function for autonomous WT systems may be unreliable. It was also seen that the ROA obtained from a system with slow current ramp rate control has a larger area when compared to the ROA from a fast ramp rate control.
3) The upper limit for the proposed energy function discussed in the paper is $[-\pi/2, +\pi/2]$. Hence, when the damping is very high for the system, the boundary $\delta_{\phi=0}$ tends to $\pm\pi/2$. As a result, the ROA is

always conservative. However, even with the conservative estimate of ROA, the results showed that the system is highly oscillatory when the post-fault initial point trajectory is near the estimated boundary. Hence, estimating a larger boundary may not be beneficial as a more oscillatory response may not be valuable. This understanding is especially true when the ROA estimate is used to tune the PLL gains.

4) From time-domain simulations, it is verified that as long as the post-fault initial point trajectory is within the estimated ROA, the energy is always positive except at equilibrium, where it is zero. Moreover, during this period, the energy change rate is always negative.

While the primary focus of this work is on individual wind turbines. It must be noted that our proposed method has the potential for adaptability at the wind power plant (WPP) level as well, where the WPP with multiple WTs can be aggregated as a single machine equivalent, and this is a plausible future extension of our research.

REFERENCES

[1] *Global Wind Report*, GWEC, Brussels, Belgium, 2021.

[2] *Wind Electricity*, IEA, Paris, France, 2022. [Online]. Available: https://www.iea.org/reports/wind-electricity

[3] J. Ma, Y. Qiu, Y. Li, W. Zhang, Z. Song, and J. S. Thorp, "Research on the impact of DFIG virtual inertia control on power system small-signal stability considering the phase-locked loop," *IEEE Trans. Power Syst.*, vol. 32, no. 3, pp. 2094–2105, May 2017, doi: 10.1109/TPWRS.2016.2594781.

[4] J. Hu, Q. Hu, B. Wang, H. Tang, and Y. Chi, "Small signal instability of PLL-synchronized type-4 wind turbines connected to high-impedance AC grid during LVRT," *IEEE Trans. Energy Convers.*, vol. 31, no. 4, pp. 1676–1687, Dec. 2016, doi: 10.1109/TEC.2016.2577606.

[5] F. Wu, X. P. Zhang, K. Godfrey, and P. Ju, "Small signal stability analysis and optimal control of a wind turbine with doubly fed induction generator," *IET Gener., Transmiss. Distrib.*, vol. 1, no. 5, pp. 751–760, Sep. 2007, doi: 10.1049/iet-gtd:20060395.

[6] H. Liu and J. Sun, "Voltage stability and control of offshore wind farms with AC collection and HVDC transmission," *IEEE J. Emerg. Sel. Topics Power Electron.*, vol. 2, no. 4, pp. 1181–1189, Dec. 2014, doi: 10.1109/JESTPE.2014.2361290.

[7] P.-H. Huang, M. S. El Moursi, W. Xiao, and J. L. Kirtley, "Subsynchronous resonance mitigation for series-compensated DFIG-based wind farm by using two-degree-of-freedom control strategy," *IEEE Trans. Power Syst.*, vol. 30, no. 3, pp. 1442–1454, May 2015, doi: 10.1109/TPWRS.2014.2348175.

[8] M. Amin and M. Molinas, "Understanding the origin of oscillatory phenomena observed between wind farms and HVdc systems," *IEEE J. Emerg. Sel. Topics Power Electron.*, vol. 5, no. 1, pp. 378–392, Mar. 2017, doi: 10.1109/JESTPE.2016.2620378.

[9] Y. Li, X. Wang, J. Guo, H. Wu, B. Zhao, S. Wang, G. Wu, and T. Wang, "PLL synchronization stability analysis of MMC-connected wind farms under high-impedance AC faults," *IEEE Trans. Power Syst.*, vol. 36, no. 3, pp. 2251–2261, May 2021, doi: 10.1109/TPWRS.2020.3025917.

[10] S. L. Brunton, B. W. Brunton, J. L. Proctor, and J. N. Kutz, "Koopman invariant subspaces and finite linear representations of nonlinear dynamical systems for control," *PLoS ONE*, vol. 11, no. 2, Feb. 2016, Art. no. e0150171, doi: 10.1371/journal.pone.0150171.

[11] T. L. Vu and K. Turitsyn, "Lyapunov functions family approach to transient stability assessment," *IEEE Trans. Power Syst.*, vol. 31, no. 2, pp. 1269–1277, Mar. 2016, doi: 10.1109/TPWRS.2015.2425885.

[12] D. J. Hill, I. A. Hiskens, and I. M. Y. Mareels, "Stability theory of differential/algebraic models of power systems," *Sadhana*, vol. 18, no. 5, pp. 731–747, Sep. 1993, doi: 10.1007/BF03024222.

[13] Z. Tian, Y. Tang, X. Zha, J. Sun, M. Huang, X. Fu, and F. Liu, "Hamilton-based stability criterion and attraction region estimation for grid-tied inverters under large-signal disturbances," *IEEE J. Emerg. Sel. Topics Power Electron.*, vol. 10, no. 1, pp. 413–423, Feb. 2022, doi: 10.1109/JESTPE.2021.3076189.

[14] *Offshore-Netzanschlussregeln (O-NAR)*, TenneT TSO, Arnhem, The Netherlands, Aug. 2019.

[15] S. Ghosh, M. K. Bakhshizadeh, G. Yang, L. Kocewiak, and B. Pal, "Nonlinear stability boundary assessment of offshore wind power plants under large grid disturbances," in *Proc. 21st Wind Sol. Integr. Workshop (WIW)*, Oct. 2022, pp. 317–324, doi: 10.1049/icp.2022.2770.

[16] L. Harnefors, X. Wang, A. G. Yepes, and F. Blaabjerg, "Passivity-based stability assessment of grid-connected VSCs—An overview," *IEEE J. Emerg. Sel. Topics Power Electron.*, vol. 4, no. 1, pp. 116–125, Mar. 2016, doi: 10.1109/JESTPE.2015.2490549.

[17] Y. Gu, N. Bottrell, and T. C. Green, "Reduced-order models for representing converters in power system studies," *IEEE Trans. Power Electron.*, vol. 33, no. 4, pp. 3644–3654, Apr. 2018, doi: 10.1109/TPEL.2017.2711267.

[18] D. Dong, B. Wen, D. Boroyevich, P. Mattavelli, and Y. Xue, "Analysis of phase-locked loop low-frequency stability in three-phase grid-connected power converters considering impedance interactions," *IEEE Trans. Ind. Electron.*, vol. 62, no. 1, pp. 310–321, Jan. 2015, doi: 10.1109/TIE.2014.2334665.

[19] H. Geng, L. Liu, and R. Li, "Synchronization and reactive current support of PMSG-based wind farm during severe grid fault," *IEEE Trans. Sustain. Energy*, vol. 9, no. 4, pp. 1596–1604, Oct. 2018, doi: 10.1109/TSTE.2018.2799197.

[20] M. K. Bakhshizadeh, S. Ghosh, Ł. Kocewiak, and G. Yang, "Improved reduced-order model for PLL instability investigations," *IEEE Access*, early access, Jul. 12, 2023, doi: 10.1109/ACCESS.2023.3294818.

[21] S. Ghosh, G. Yang, M. K. B. Dowlatabadi, and L. Kocewiak, "Nonlinear stability analysis of a reduced-order wind turbine VSC-grid model operating in weak grid conditions," in *Proc. 20th Int. Workshop Large-Scale Integr. Wind Power Power Syst. Well Transmiss. Netw. Offshore Wind Power Plants (WIW)*, Sep. 2021, pp. 457–463, doi: 10.1049/icp.2021.2649.

[22] L. Kocewiak, R. Blasco-Giménez, C. Buchhagen, J. B. Kwon, Y. Sun, A. S. Trevisan, M. Larsson, and X. Wang, "Overview, status and outline of stability analysis in converter-based power systems," in *Proc. 19th Int. Workshop Large-Scale Integr. Wind Power Power Syst.* Darmstadt, Germany: Energynautics, Nov. 2020, pp. 11–12.

[23] Y. Lu, Z. Du, Y. Li, and Y. Zhang, "Nonlinear damping property and limit cycle of VSC," *IEEE Trans. Power Del.*, vol. 37, no. 5, pp. 4485–4488, Oct. 2022, doi: 10.1109/TPWRD.2022.3181852.

[24] H. Choi, P. J. Seiler, and S. V. Dhople, "Robust power systems stability assessment with sum of squares optimization," in *Proc. IEEE Power Energy Soc. Gen. Meeting*, Jul. 2015, pp. 1–5, doi: 10.1109/PESGM.2015.7286245.

[25] H.-D. Chang, C.-C. Chu, and G. Cauley, "Direct stability analysis of electric power systems using energy functions: Theory, applications, and perspective," *Proc. IEEE*, vol. 83, no. 11, pp. 1497–1529, Nov. 1995, doi: 10.1109/5.481632.

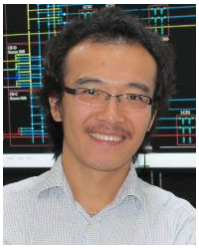
[26] J. W. Baker, "Stability properties of a second order damped and forced nonlinear differential equation," *SIAM J. Appl. Math.*, vol. 27, no. 1, pp. 159–166, Jul. 1974, doi: 10.1137/0127013.



SUJAY GHOSH (Graduate Student Member, IEEE) received the M.Sc. degree in electrical engineering from the Technical University of Denmark (DTU). He is currently pursuing the Ph.D. degree in the stability of large renewable power plants in low inertia systems with DTU in collaboration with Ørsted Wind power A/S. He was a system studies engineer in the electrical industry in India and Denmark. His current research interest includes power system stability and control.



MOHAMMAD KAZEM BAKHSHIZADEH received the B.S. and M.S. degrees in electrical engineering from the Amirkabir University of Technology, Tehran, Iran, in 2008 and 2011, respectively, and the Ph.D. degree from Aalborg University, Aalborg, Denmark, in 2018. In 2016, he was a Visiting Scholar with Imperial College London, London, U.K. He is currently a Senior Power System Engineer with Ørsted Wind Power, Fredericia, Denmark. His current research interests include power quality, modeling, control and stability analysis of power converters, and grid converters for renewable energy systems.



GUANGYA YANG (Senior Member, IEEE) joined the Technical University of Denmark (DTU), in 2009, where he is currently a Senior Scientist with the Department of Wind and Energy Systems. Previously, he was a full-time employee with Ørsted, where he is focusing on the electrical design of large offshore wind farms. He has received numerous research grants, including the recent H2020 MSCA ITN Project InnoCyPES as a Coordinator. His current research interests include the stability, control, and operation of power systems. He is a member of the IEC Technical Committee ''Wind Power Generation Systems'' (TC88) and the Convenor of IEC61400-21-5. He is currently serving as a Lead Editor for IEEE Access of the Power and Energy Society Section and has been an editorial board member for several journals.



ŁUKASZ KOCEWIAK (Senior Member, IEEE) received the B.Sc. and M.Sc. degrees in electrical engineering from the Warsaw University of Technology, in 2007, and the Ph.D. degree from Aalborg University, in 2012. Currently, he is with Ørsted as the Research and Development Manager. He is a power system specialist in the area of design of electrical infrastructure in large offshore wind power plants. He is the author/co-author of more than 100 publications. His current research interests include harmonics, stability, and nonlinear dynamics in power electronics and power systems especially focused on wind power generation units. He is a member of various working groups/activities within Cigré and IEC.



BIKASH C. PAL (Fellow, IEEE) received the B.E.E. degree (Hons.) in electrical engineering from Jadavpur University, Calcutta, India, in 1990, the M.E. degree in electrical engineering from the Indian Institute of Science, Bengaluru, India, in 1992, and the Ph.D. degree in electrical engineering from Imperial College London, London, U.K., in 1999. Currently, he is a Professor with the Department of Electrical and Electronic Engineering, Imperial College London. His current research interests include renewable energy modeling and control, state estimation, and power system dynamics. He is the Vice President of Publications of the IEEE Power and Energy Society. He was the Editor-in-Chief of IEEE Transactions on Sustainable Energy, from 2012 to 2017, and *IET Generation, Transmission and Distribution*, from 2005 to 2012.



MITHULAN NADARAJAH (Senior Member, IEEE) received the B.Sc. (Eng.) degree from the University of Peradeniya, Sri Lanka, in May 1993, the M.Eng. degree from the Asian Institute of Technology (AIT), Bangkok, Thailand, in August 1997, and the Ph.D. degree from the University of Waterloo, ON, Canada. Prior to joining The University of Queensland, in 2009, he was with the Energy Field of Study, AIT. He was a Planning Engineer with the Generation Planning Division, Ceylon Electricity Board (CEB), Sri Lanka, and a Project Leader with the Centre of Excellence in Electric Power Technology (CEEPT), Chulalongkorn University, Thailand.